HHS Public Access

Author manuscript

ACS Nano. Author manuscript; available in PMC 2019 February 27.

Published in final edited form as:

ACS Nano. 2018 February 27; 12(2): 1508–1518. doi:10.1021/acsnano.7b08044.

A Programmable DNA Origami Platform for Organizing Intrinsically Disordered Nucleoporins within Nanopore Confinement

Patrick D. Ellis Fisher[†,‡,§], **Qi Shen**[†,‡,§], **Bernice Akpinar**[⊥,∥], **Luke K. Davis**[∥,▽,○], **Kenny Kwok Hin Chung**[†,‡], **David Baddeley**[†,‡], **Anđela Šarić**[▽,○], **Thomas J. Melia**[†], **Bart W. Hoogenboom**[∥,▽,○], **Chenxiang Lin**[*,†,‡], and **C. Patrick Lusk**[*,†]

[†]Department of Cell Biology, Yale School of Medicine, New Haven, Connecticut 06520, USA

[‡]Nanobiology Institute, Yale University, West Haven, Connecticut 06516, USA

[⊥]Department of Chemistry, Imperial College London, London, SW7 2AZ, UK

[∥]London Centre for Nanotechnology, University College London, 17–19 Gordon Street, London WC1H 0AH, UK

[▽]Department of Physics and Astronomy, University College London, Gower Street, London WC1E 6BT, UK

[○]Institute for the Physics of Living Systems, University College London, Gower Street, London WC1E 6BT, UK

Abstract

Nuclear pore complexes (NPCs) form gateways that control molecular exchange between the nucleus and the cytoplasm. They impose a diffusion barrier to macromolecules and enable the selective transport of nuclear transport receptors with bound cargo. The underlying mechanisms that establish these permeability properties remain to be fully elucidated, but require unstructured nuclear pore proteins rich in Phe-Gly (FG)-repeat domains of different types, such as FxFG and GLFG. While physical modeling and *in vitro* approaches have provided a framework for explaining how the FG network contributes to the barrier and transport properties of the NPC, it remains unknown whether the number and/or the spatial positioning of different FG-domains along a cylindrical, ~40 nm diameter transport channel contributes to their collective properties and function. To begin to answer these questions, we have used DNA origami to build a cylinder that mimics the dimensions of the central transport channel and can house a specified number of FG-domains at specific positions with easily tunable design parameters, such as grafting density and topology. We find the overall morphology of the FG-domain assemblies to be dependent on their chemical composition, determined by the type and density of FG-repeat, and on their architectural confinement provided by the DNA cylinder, largely consistent with here presented molecular dynamics simulations based on a coarse-grained polymer model. In addition, high-speed atomic force microscopy reveals local and reversible FG-domain condensation that

Correspondence to: Chenxiang Lin: chenxiang.lin@yale.edu or C. Patrick Lusk: patrick.lusk@yale.edu.

[§]These authors contributed equally to this work; position determined by coin toss.

transiently occludes the lumen of the DNA central channel mimics, suggestive of how the NPC might establish its permeability properties.

Keywords

nuclear pore complex; nucleoporins; nuclear transport; intrinsically disordered proteins; DNA nanotechnology; DNA origami; DNA-directed self-assembly

Nuclear pore complexes (NPCs) form gateways in the nuclear envelope that control molecular traffic between the cytoplasm and the nucleus. There are thousands of NPCs on a mammalian cell nucleus, which enable a substantial flux of transcription factors, histones, mRNPs and ribosomal subunits. Its transport properties are essential for the spatial segregation of the gene expression machinery in eukaryotes. To establish and maintain two biochemically distinct compartments, the NPC imposes a size-selective diffusion barrier to macromolecules as small as ~5 nm while simultaneously promoting the translocation of nuclear transport receptor (NTR; karyopherins, importins, exportins)-bound cargos, some of which are large enough to span the ~40 nm-diameter channel.[1] The molecular mechanisms that establish these permeability properties remain to be fully understood.

Such understanding is greatly hampered by the disordered nature of a subset of ~12 nuclear pore proteins, termed nucleoporins or "nups," rich in Phe-Gly (FG) amino acid residues. These "FG-nups" fill the NPC transport channel with thousands of repetitive peptide motifs like FxFG, GLFG, and PSFG that together establish the NTR-selective and diffusion-barrier properties of the NPC[2–16] and also help hold the NPC together.[17] However, as the FG-network is refractory to traditional structure-based experimental approaches, its organization has remained ill-defined. This contrasts with the 8-fold radially symmetric NPC scaffold, which is now visualized with sufficient resolution in cryo-EM maps to allow docking of crystal structures of nups[18, 19] that constitute the major inner and outer ring complexes,[20–23] as well as aspects of the cytosolic-facing mRNA export platform.[24] These structures, in combination with extensive biochemical analyses of nup-nup interactions[25–29] and nup stoichiometry[21, 25, 26, 30, 31] are revealing the fundamental and evolutionarily conserved mechanisms that construct the NPC, but have not yet been able to fully define its permeability properties.

Efforts to directly examine the FG-network *in vivo* (or *ex vivo* within purified nuclear envelopes from *Xenopus* oocytes) have relied on fluorescence microscopy[32–34] and atomic force microscopy (AFM),[35, 36] but these strategies are only sensitive to a small subset of proteins in the NPC (fluorescence) or to overall protein content without chemical identification (AFM). Thus, understanding the biophysical properties of the FG-network has largely relied on *in vitro* approaches, where FG-nups exhibit collective forms that bridge between hydrogels[7, 9, 11, 37] and entropically governed polymer brushes.[38–40] Considerable debate continues over the functional relevance of intermolecular attractive FG-nup interactions, dubbed "cohesivity",[7, 8, 11, 15, 41–45] that can cause the FG-nups to toggle between these two morphological extremes and is a central component of some, but not all, transport models.[13, 38, 46–50]

Efforts have also been directed at explaining FG-nup behavior within conceptually simple polymer models that ignore many of the underlying chemical details of the FG-nups.[40, 51] These models can explain the behavior of FG-nups grafted onto planar films, which is impacted by the type of FG-nup, grafting density, and the concentration of NTRs in solution.[43, 45, 49, 52] However, such polymer models[53, 54] also predict qualitatively different collective behaviors depending on the exact architecture and geometry that the FG-nups are grafted in. These predictions remain to be fully explored experimentally.

Hence, important outstanding questions include: how FG-nups organize within nanopore confinements that mimic the NPC channel, how this organization depends on the grafting geometry, density and stoichiometry, how it depends on the type of FG-nup—given that not all FG-nups are alike[55]—and to what extent such behaviors can be captured by generic polymer physics. Ideally, this is explored in a system that also offers a perspective to investigate how such behaviors translate into transport properties in a pore geometry. Encouragingly, NPC transport properties have been recapitulated in nanopore devices containing grafted FG-nups,[56, 57] although those devices provided limited control over and experimental access to the underlying FG-nup behavior.

In this work, we use DNA nanotechnology,[58] specifically the technique termed “DNA origami,” which can fold a long, single-stranded DNA (ssDNA) into specifically designed shapes.[59, 60] DNA origami is particularly useful for building nanoscale scaffolds capable of organizing guest molecules with precisely controlled stoichiometry and spatial positioning. For example, a defined number (usually less than 10) of well-folded proteins, such as SNAREs,[61] motor proteins,[62, 63] enzymes,[64] and ephrins,[65] have been assembled on DNA origami structures. Here, we employ DNA origami to construct biomimetic nanopores where FG-nup anchor points and stoichiometry can be precisely controlled within native NPC geometry. We provide evidence that cylindrical confinement impacts the collective properties of FG-nups while establishing an experimental system that allows the direct visualization of FG-nup dynamics within pore architectures.

RESULTS AND DISCUSSION

Generation of NucleoPorins Organized on DNA (NuPOD)

To mimic the native ~40 nm NPC channel,[20] we designed a DNA origami cylinder with an inner diameter of 46 nm and a height of 14 nm (Figure 1a). The cylinder consists of 16 DNA double helices and contains 21-nucleotide ssDNA handles that extend inward from the inner wall in up to four layers, providing anchor points for the FG-nups (Figures 1a and S1). These handles are flexible; when annealed with the complementary anti-handles, they will form 7 nm long double-stranded DNA rods that can rotate around their anchor points at the DNA origami cylinder. Hence the effective diameter of the FG-nup grafting points inside the DNA origami will range between 32 and 46 nm (Figure 1a).

Most of our DNA cylinders mimic the 8-fold symmetry of the NPC and contain 8, 16, 24, or 32 FG nups arranged in 1 to 4 layers of 8, respectively. However, to accommodate 48 proteins (corresponding to the number of Nsp1 in the budding yeast NPC),[25, 26] the number of anchor points per layer must be increased to 12 to satisfy design constraints imposed by

the limiting length of the scaffold strand. The 48-handle DNA cylinder has a grafting density of ~3 FG-nup molecules per 100 nm^2, which is comparable to previously-studied planar monolayers of FG-nups[43, 45, 49, 51, 52] and can house FG-repeats at physiologically relevant concentrations (100–200 mM).[16, 30, 66]

We functionalized the DNA origami cylinders with purified FG-domains derived from *S. cerevisiae* Nsp1 and Nup100 (orthologues of metazoan Nup62 and Nup98) as representatives of the two major FxFG and GLFG repeat classes, respectively (Figure 1b). Importantly, these FG-domains have virtually identical molecular masses but have distinct chemical composition in their amino acid sequences (Table S1). The FG-domains were recombinantly expressed with a TEV-cleavable 10×His-MBP-SUMO tag[8] to ensure solubility in physiological buffers (Figure 1b and Table S1). To incorporate FG-domains into the DNA cylinder in the correct orientation (*i.e.*, anchored at their C-termini),[67–69] we chemically conjugated them to maleimide-modified DNA anti-handles (21-nucleotide strands complementary to the handles) *via* an engineered C-terminal cysteine, producing a site-specific, stoichiometric protein-DNA conjugate (Figure 1c). The FG-domains were incorporated into the cylinder by hybridizing the handles and anti-handles to generate what we term Nucleoporins Organized on DNA, or "NuPODs." The NuPODs used for all subsequent experiments were purified by rate-zonal centrifugation, which separated NuPODs from free proteins (Figure 1d).

Quality control of NuPODs

To ensure that purified NuPODs with 1–48 handles housed the predicted number of FG-domains, we first analyzed them by SDS-agarose gel electrophoresis (SDS-AGE). As anticipated, the increase in polypeptide copy number led to a corresponding gel mobility shift (Figure 2a). Moreover, at least the MBP-Nup100 containing NuPODs were resolved as single bands, indicating that these samples were homogenous; MBP-Nsp1 NuPODs were slightly more diffuse (Figure S2). We next loaded equivalent amounts of NuPODs onto SDS-PAGE gels and immunoblotted for the 10×His tag. By comparing signal intensities to an internal FG-nup concentration standard curve, we determined that there was a quantitative agreement with the design prediction, for example, the 48-handle NuPOD had 45.1 ± 5.2 (mean ± SD) copies of MBP-Nup100 (Figures 2b, S2, and Table S2). We also performed immunoblots on samples normalized to the concentration of DNA handles and thus theoretically, to the concentration of FG-nups. Consistent with this idea, the signal intensity was comparable between samples (Figures 2b and S2).

GLFG and FxFG domains exhibit distinct morphologies in NuPODs

To visualize the morphology of the FG-domains in the confinement of the DNA cylinder, we employed negative-stain transmission electron microscopy (TEM). We could only observe protein density (appearing as white clumps) in NuPODs with at least 8 copies of MBP-Nup100 (Figures 2c and S3). As the protein copy number was increased to 48, the center of the cylinder was often completely filled. We also observed filled rings with 48 copies of MBP alone but these were more likely to form a donut-shape with a lack of density in the center (Figures 3a and S4).

NuPODs with 1–24 copies of MBP-Nsp1 grafted on the inside of the DNA rings appeared similar to their cognate Nup100 variants, although were consistently more difficult to stain (Figure 2d and S5). With 48 copies, the MBP-Nsp1 extended beyond the cylinder, as evidenced by many white puncta surrounding the outside of the ring (exemplified by arrowheads in Figure 2d); it is reasonable to consider these puncta to be the MBP moieties.

To help interpret our experimental observations, we performed coarse-grained molecular dynamics simulations for the respective grafting geometries (Figure 2c,d, lower panels). In these simulations, Nup100-FG and Nsp1-FG were modeled as homogenous polymers that experienced volume-exclusion as well as attractive intra-/intermolecular interactions. Under the conditions and in particular the salt concentrations that apply in our experiments, electrostatic effects are known to be screened within ~2 nm of the DNA,[70] *i.e.*, a small range compared with the experimentally observed locations of the FG-domains. Hence, beyond the attachment at the grafting points, volume-exclusion was presumed to be the only relevant interaction between the FG-nups and the DNA scaffold. The strength of the attractive, also termed "cohesive",[45] interaction between the polymers was set by comparing computational and experimental data for FG-nup assemblies that were grafted in planar geometry (Figure S6 and described in SI), in a conceptual approach that we had previously found successful in describing the morphology of FG-nup films and their uptake of NTRs.[51]

The resulting FG-nup arrangements in the MD simulations appear in good overall agreement with the TEM data, notably in the distributions of the MBP domain (grey spheres in the MD snapshots in Figure 2c,d) as a function of FG-nup copy number, and specifically in the larger spread of the Nsp1 variant in the 48-handle system, compared with Nup100. This difference between the Nsp1 and Nup100 FG-domains is fully consistent with previous reports[43, 45] and indeed with the data underpinning the parameter settings for these simulations,[51] showing Nsp1 to be less cohesive than Nup100 (or its metazoan orthologue Nup98), and thus able to occupy a greater volume. Simulations with and without the terminal MBP yielded largely similar results (Figures 2c,d and S7), indicating that the presence of the (inert) MBP—while beneficial for highlighting the presence of proteins attached to the NuPODs—did not greatly affect the FG-nup morphology in the NuPODs.

3D architecture influences FG-nup morphology

Given the prediction from polymer models that pore geometry is a major determining factor for FG-nup behavior and particular compaction in the NPC,[53, 54] we next compared NuPODs with 48 copies of MBP-Nup100 or MBP-Nsp1 grafted on the inside and outside of the DNA cylinder, annotated as 48×MBP-Nup100(in) or (out) (Figure 3a). As determined from the cylinder dimensions, the inside *versus* outside grafting corresponds to a difference in grafting density of only ~30%. Notably, as discussed above, we found that pore confinement facilitates central condensation of the FG-nups, in particular for the 48×MBP-Nup100(in) and to a lesser extent for 48×MBP-Nsp1(in) (Figure 3a). On the other hand, grafting of both FG-domains on the outside of the rings resulted in the appearance of an extended radial array of fibers culminating in white puncta (the MBP). Interestingly, the Nup100-FG domains consistently extended as far, if not slightly further, than the Nsp1-FG domains (Figure 3a,c). This was surprising, as the MD simulations for the outside-grafted

NuPODs yielded protein distributions that were slightly more compact than their extended appearance in the TEM data (Figure 3b), consistent with the idea that they are more cohesive. We recognize that this potential discrepancy might be due to surface dehydration effects inherent in negative-stain TEM preparations; however, a similar trend was observed using single-molecule switching (SMS) super-resolution microscopy (Figure 3d,e), where the MBP-FG-domains were labeled with a primary anti-MBP and a secondary Alexa-647-conjugated antibody. In these experiments, we observed antibody-induced condensation of the Nup100/Nsp1-FG-domains grafted on the outside of the rings (Figure S8b), yet still leaving the MBP-Nup100 localization cloud more dispersed than that of MBP-Nsp1 (Figure 3d,e).

Lastly, to avoid surface and antibody-induced effects on FG-nup behavior, we examined the NuPODs using dynamic light scattering (DLS), with the caveat that the DLS size estimates assume that NuPODs scatter light as spherical particles. Gratifyingly, both MBP-Nup100(in) and MBP-Nsp1(in) NuPODs had little impact on average size measurements when compared with MBP-only controls (Figure 3f). With FG-nups anchored to the outside of the DNA cylinder, the measured NuPOD sizes were larger and showed a wider size distribution (*i.e.*, less homogenous; note the logarithmic scaling of the horizontal axis), suggesting less condensed and/or more heterogeneous assembly states of those outward-facing FG-nups, consistent with the coarse-grained MD results (Figure 3b). Interestingly, and consistent with the TEM and super-resolution data, DLS measurements showed a larger apparent diameter for 48×MBP-Nup100(out) than for 48×MBP-Nsp1(out), indicating that the collective behavior of Nup100-FG domains might be sensitive to grafting orientation. These data suggest that Nup100 condensation might be preferred upon assembly within a NPC-like cylinder.

FG-nups appear condensed yet dynamic within the NuPOD architecture

For label-free and high-resolution measurements of FG-nup morphology in solution, we imaged NuPODs by atomic force microscopy (AFM). In these experiments, NuPODs were adsorbed on a supported lipid bilayer (Figure 4a), the composition of which was optimized to facilitate NuPOD adsorption (through charge-charge interactions[71–73]) while minimizing the interactions of the FG-nups with the AFM substrate (Figure S9 and described in SI). At low magnification, the AFM topography revealed a diffuse filling in the majority of the pores for 48×MBP-Nup100(in) and 48×MBP-Nsp1(in) (Figure 4b,c), consistent with the TEM and MD results. A quantification of this filling was complicated by the invasiveness of the AFM imaging; for AFM imaging forces just beyond a minimum of the order of 0.1 nN (see SI), the NuPODs appeared mostly empty (Figure S10), indicating that the FG-nups were at the detection limit of these AFM experiments. NuPODs were also characterized following cleavage of the MBP at the free end of the FG nups (Figure S11 and described in SI), yielding an overall somewhat poorer reproducibility in the appearance of the NuPOD lumen (Figure S12), most likely due to the absence of the more readily detected MBP domains.

At higher magnification (Figure 4d), AFM clearly resolved attached protein for 48×MBP(in) and 48×MBP(out), indicating that the DNA handles were robust under the AFM imaging.

The presence of protein inside the rings was also evident for 48×MBP-Nup100(in) and 48×MBP-Nsp1(in), but only few clumps of protein were detected for the NuPODs with the FG-nups grafted at the outside of the DNA rings, *i.e.*, 48×MBP-Nup100(out) and 48×MBP-Nsp1(out) (Figure 4d, also see line profiles below images). This again suggests that the FG-nups were too flexible and/or mobile to be fully resolved by AFM, but that they did appear in the AFM images when they maintained sufficient local condensation.

As we observed some variability in the relative "filling" of the NuPOD lumens (Figure 4b,c), we next performed AFM on 48×MBP-Nup100(in) and 48×MBP-Nsp1(in) NuPODs, as well as their MBP-cleaved counterparts, 48×Nup100(in) and 48×Nsp1(in), as a function of time (Figure 5a and Videos S1–4). To assess the robustness of the AFM data and measurement process, we systematically recorded both trace and retrace images (*i.e.*, left-to-right and right-to-left line scans, Figure S13 and described in SI). These measurements show that the topographic features of the NuPODs were largely reproducible at a time scale of 25 ms (the average time between trace and retrace line scans in our experiments). However, from image to image of the entire NuPOD (captured every ~1.6 s), significant changes within the NuPOD lumen were observed that were qualitatively similar for both MBP-Nup100 and MBP-Nsp1 as well as for (though studied less comprehensively) outside-grafted systems (Video S5). Most strikingly, we observed local enhancements of protein density that shifted position as time evolved and often appeared to extend and make contact with analogous densities emanating from multiple positions along the channel walls. As predicted by MD simulations, the behavior of the FG-nups was not appreciably affected by removal of the MBP moieties (Figure 5a, Videos S2 and S4).

To further resolve the FG-nup behavior at higher temporal resolution, we repeatedly scanned the same line across a single NuPOD (Figure 5b, dotted line; Figure S14). We plotted trace and retrace line profiles separately as a reproducibility check as before, with subsequent scan lines separated by 2 × 25 ms = 50 ms. With the evolved time on the horizontal axis, we obtained kymographs that highlight changes in FG-nup arrangements at ~1 s time scale (Figure 5c, as explained in Video S6). FG-nup densities can be observed transiently and stochastically throughout the kymograph (see also line profiles at indicated positions, Figure 5d) that span the two sides of the ring. Together, these data support that locally condensed FG-domains are dynamic and can make reversible interactions that span and could temporally occlude a ~40 nm channel.

CONCLUSIONS

We have taken a bottom-up engineering approach to examine the collective properties of precise numbers of FG-nups that are confined within a cylindrical architecture mimicking the geometry of the native NPC channel (Figure 1). This has enabled a direct experimental investigation of how FG-nup cohesiveness and dynamic behavior emerge within a nanopore confinement with physiologically relevant numbers of FG-nups, and of how these may ultimately translate into the formation of the natural NPC permeability barrier.

While the data presented here do not directly address the establishment of a permeability barrier inside the NuPODs, it is nonetheless tempting to interpret our observations within

this context. First, it is clear that 48 copies of either FG-nup are capable, in principle, of occluding a 40 nm diameter channel. Most strikingly, however, is that the FG-nups can undergo local and reversible condensation, including transitions from pore-occluding to more open configurations (Figure 5 and Videos S1–4). These AFM experiments must be interpreted with the caveat that more mobile and/or diffuse FG-nup arrangements may not be fully resolved because of the inherent invasiveness of the AFM measurement. However, the here shown NuPOD (and FG-nup) topographies are robust, as inferred from the good reproducibility between trace and retrace line profiles (see, *e.g.*, Fig. 5c). Hence, these results imply FG-nup condensation as expected for gel/selective-phase models[7, 46] as well as —at the nanometer length scale—dynamics that are in line with descriptions that emphasize entropy-dominated behavior.[38, 49] These data are also consistent with earlier speculations on how such rearrangements may facilitate selective transport across the NPC[54] and thus provide a conceptual framework to consider how the native NPC might allow translocation of large macromolecules while also imposing a "soft" diffusion barrier.[74–76]

Given this physiological context of FG-nups, it is also worthwhile to compare the NuPOD data with recent AFM experiments on intact *Xenopus laevis* NPCs.[35, 36] Firstly, the NuPOD lumens appear more diffuse and mechanically less robust than NPC lumens, implying that the filled and highly cohesive appearance of NPC lumens[35] may at least partially be due to the presence of NTRs in the native FG-nup network.[49, 56, 77] Conveniently, this emptier appearance of the NuPODs greatly facilitates the study of collective FG-nup dynamics: The height fluctuations in the NuPOD lumens are observed at the scale of 1–10 nm (Figure 5, and highlighted in Figure 5d specifically), up to an order of magnitude above the height fluctuations observed at a similar time scale by AFM in NPC lumens (and interpreted as due to individual FG nups).[36] These height fluctuations in the NuPODs are well above the AFM noise floor, facilitating their identification as *bona fide* representations of FG-nup dynamics.

The coarse-grained MD simulations facilitated the interpretation of our experimental data in terms of FG-nup morphology within the NuPODs. While computational simulations may take into account chemical heterogeneity within FG-nups,[78, 79] we obtain a good agreement with protein distributions in the TEM images by modeling the FG-nups as homogeneous polymers that experience an overall attractive (or "cohesive") inter- and intramolecular interaction (Figure 2c,d). This agreement between experiment and simulations includes the wider spread of Nsp1 compared with the more cohesive Nup100 for the 48-handle inside grafted NuPODs. It indicates that the collective FG-nup morphology can largely be understood using rather generic polymer physics, ignoring many of the underlying chemical and structural details. This conclusion is fully consistent with recent observations based on experiments with FG-nups grafted in a planar geometry.[40, 45, 51, 80]

Those prior experiments on planar, 2D surfaces were unable, however, to address how FG-nup confinement within a cylindrical architecture impacts their collective behavior. This concept is best exemplified by the potentially interesting difference in morphology of the Nup100 FG-domains when grafted on the inside *versus* the outside of the DNA cylinder (Figure 3). Pore confinement appears to enhance the condensation of Nup100, confirming predictions from polymer physics;[53, 54] but when grafted on the outside of the NuPOD cylinder, the Nup100 FG-domains extend over a considerably larger area. More puzzling,

however, we find that the outside-grafted Nup100 extends further than the outside-grafted Nsp1 despite overwhelming evidence that it is more cohesive than Nsp1.[45, 48, 49, 51] This is a small difference in the TEM data (Figure 3c), but is also observed by localization microscopy (SMS) and DLS (Figure 3d–f), which makes it difficult to ignore. While the nature of the observed differences between outside-grafted Nup100 and Nsp1 remains to be explained, our data overall suggest that these GLFG and FxFG-rich nups have biophysical/biochemical properties that are clearly influenced by grafting density and cylindrical confinement.

Taken together, our first-generation NuPODs introduce a powerful and flexible experimental system to probe the biophysical properties of FG-nups within cylindrical architectures that mimic the NPC channel. Although in this work we focused on proof-of-concept demonstration using two types of FG-nups, the platform presented here can be applied to organize other FG-nups or other intrinsically disordered proteins capable of phase separation, thus presenting opportunities to generate more sophisticated and diverse biomimetic constructs. In that sense, the NuPOD platform helps extend the applications of DNA nanotechnology to both cell biology (*in vitro* modeling of nuclear transport) and synthetic biology (designing macromolecule sorters with tunable selectivity). Indeed, this study highlights the power of the DNA origami technique to build synthetic macromolecular structures with biologically relevant numbers (and concentrations) of proteins; the future goal of such designs is to reconstitute a fully synthetic NPC mimic in a configuration that also facilitates transport measurements.

METHODS

Extended methods are available in the Supporting Information.

NuPOD Assembly

DNA origami was designed and assembled using established techniques (see SI). 5'-amino-labeled ssDNA anti-handles were ordered from Integrated DNA Technologies and reacted with 10-fold molar excess of sulfo-SMCC and purified by ethanol precipitation. Sulfo-SMCC-reacted DNA (referred to as maleimide-DNA) was mixed in 5-fold molar excess with purified cysteine-terminated, MBP-tagged FG-nups, incubated at 37°C for 3 hr, and purified using size exclusion chromatography. DNA-labeled FG-nups were mixed in 7.5-fold excess (over the handle number) to DNA origami cylinders and incubated at 37°C for 3 hr, then purified by rate-zonal centrifugation through a glycerol gradient.

Transmission Electron Microscopy (TEM)

Negative staining for TEM was performed by depositing 5 μl sample on a glow-discharged formvar/carbon coated copper grid (Electron Microscopy Sciences) and staining with 2% uranyl formate. Imaging was performed on a JEOL JEM-1400 Plus microscope operated at 80 kV with a bottom-mount 4k×3k CCD camera (Advanced Microscopy Technologies).

Single-Molecule Switching Microscopy

NuPODs immunolabeled with anti-MBP (murine IgG2A; New England Biolabs) were laid down onto streptavidin-coated coverslips through BSA-biotin linkages on one side of the NuPOD and mounted in custom-made sealed chambers,[81] followed by labeling with Alexa 647-conjugated secondary antibodies. Stochastic Optical Reconstruction Microscopy (STORM) data was acquired and images were rendered using jittered triangulation.[82] Individual NuPODs were segmented by choosing a threshold such that 90% of the total signal was contained within the segmented objects. See details in SI.

Atomic Force Microscopy

Supported lipid bilayers (SLB) were prepared following procedures described in SI and elsewhere,[83] using 1,2-dihexadecanoyl-*sn*-glycero-3-phosphocholine (DPPC; zwitterionic head group) and dimethyldioctadecylammonium bromide salt (DDAB; cationic head group) at a 3:1 molar ratio. NuPODs were then added to this positively-charged, gel-phase SLB. AFM measurements were performed in liquid (see details in SI).

Molecular Dynamics Simulations

Coarse-grained MD simulations were performed using the LAMMPS package,[84] as detailed in SI, with the FG-nup proteins modeled as homogeneous bead-spring polymers and the MBPs as spheres. All particles in the system experienced excluded-volume interactions; in addition, the FG-nups interacted *via* an attractive potential of a strength that was set by comparison of the experimental and computational thicknesses for films of relevant FG-nups, as described previously[51] (Figure S6).

Supplementary Material

Refer to Web version on PubMed Central for supplementary material.

Acknowledgments

We thank J. Edel and members of the Lusk, Lin and Hoogenboom lab for discussion and acknowledge A. Pyne and R. Thorogate for support carrying out the AFM experiments.

This work was funded by the NIH (R21GM109466 to CPL, CL and TJM, DP2GM114830 to CL, RO1GM105672 to CPL, and T32GM007223 to PDEF) and the UK Engineering and Physical Sciences Research Council (EP/L015277/1, EP/L504889/1, and EP/M028100/1).

References

1. Schmidt BH, Görlich D. Transport Selectivity of Nuclear Pores, Phase Separation, and Membraneless Organelles. Trends Biochem. Sci. 2016; 41:46–61. [PubMed: 26705895]
2. Bayliss R, Ribbeck K, Akin D, Kent HM, Feldherr CM, Görlich D, Stewart M. Interaction between NTF2 and XFXFG-Containing Nucleoporins Is Required to Mediate Nuclear Import of RanGDP. J. Mol. Biol. 1999; 293:579–593. [PubMed: 10543952]
3. Rexach M, Blobel G. Protein Import into Nuclei: Association and Dissociation Reactions Involving Transport Substrate, Transport Factors, and Nucleoporins. Cell. 1995; 83:683–692. [PubMed: 8521485]

4. Bednenko J, Cingolani G, Gerace L. Importin Beta Contains a COOH-Terminal Nucleoporin Binding Region Important for Nuclear Transport. J. Cell Biol. 2003; 162:391–401. [PubMed: 12885761]
5. Chaillan-Huntington C, Braslavsky CV, Kuhlmann J, Stewart M. Dissecting the Interactions between NTF2, RanGDP, and the Nucleoporin XFXFG Repeats. J. Biol. Chem. 2000; 275:5874–5879. [PubMed: 10681579]
6. Iovine MK, Watkins JL, Wente SR. The GLFG Repetitive Region of the Nucleoporin Nup116p Interacts with Kap95p, an Essential Yeast Nuclear Import Factor. J. Cell Biol. 1995; 131:1699–1713. [PubMed: 8557738]
7. Frey S, Görlich D. A Saturated FG-Repeat Hydrogel Can Reproduce the Permeability Properties of Nuclear Pore Complexes. Cell. 2007; 130:512–523. [PubMed: 17693259]
8. Hülsmann BB, Labokha AA, Görlich D. The Permeability of Reconstituted Nuclear Pores Provides Direct Evidence for the Selective Phase Model. Cell. 2012; 150:738–751. [PubMed: 22901806]
9. Schmidt HB, Görlich D. Nup98 FG Domains from Diverse Species Spontaneously Phase-Separate into Particles with Nuclear Pore-Like Permselectivity. eLife. 2015; 4
10. Mohr D, Frey S, Fischer T, Guttler T, Görlich D. Characterisation of the Passive Permeability Barrier of Nuclear Pore Complexes. EMBO J. 2009; 28:2541–2553. [PubMed: 19680228]
11. Frey S, Görlich D. FG/FxFG as well as GLFG Repeats Form a Selective Permeability Barrier with Self-Healing Properties. EMBO J. 2009; 28:2554–2567. [PubMed: 19680227]
12. Hough LE, Dutta K, Sparks S, Temel DB, Kamal A, Tetenbaum-Novatt J, Rout MP, Cowburn D. The Molecular Mechanism of Nuclear Transport Revealed by Atomic-Scale Measurements. eLife. 2015; 4
13. Lim RYH, Fahrenkrog B, Köser J, Schwarz-Herion K, Deng J, Aebi U. Nanomechanical Basis of Selective Gating by the Nuclear Pore Complex. Science. 2007; 318:640–643. [PubMed: 17916694]
14. Milles S, Mercadante D, Aramburu IV, Jensen MR, Banterle N, Koehler C, Tyagi S, Clarke J, Shammas SL, Blackledge M, Gräter F, Lemke EA. Plasticity of an Ultrafast Interaction between Nucleoporins and Nuclear Transport Receptors. Cell. 2015; 163:734–745. [PubMed: 26456112]
15. Patel SS, Belmont BJ, Sante JM, Rexach MF. Natively Unfolded Nucleoporins Gate Protein Diffusion across the Nuclear Pore Complex. Cell. 2007; 129:83–96. [PubMed: 17418788]
16. Strawn LA, Shen T, Shulga N, Goldfarb DS, Wente SR. Minimal Nuclear Pore Complexes Define FG Repeat Domains Essential for Transport. Nat. Cell Biol. 2004; 6:197–206. [PubMed: 15039779]
17. Onischenko E, Tang JH, Andersen KR, Knockenhauer KE, Vallotton P, Derrer CP, Kralt A, Mugler CF, Chan LY, Schwartz TU, Weis K. Natively Unfolded FG Repeats Stabilize the Structure of the Nuclear Pore Complex. Cell. 2017; 171:904–917. e919. [PubMed: 29033133]
18. Schwartz TU. The Structure Inventory of the Nuclear Pore Complex. J. Mol. Biol. 2016; 428:1986–2000. [PubMed: 27016207]
19. Beck M, Hurt E. The Nuclear Pore Complex: Understanding Its Function through Structural Insight. Nat. Rev. Mol. Cell Biol. 2017; 18:73–89. [PubMed: 27999437]
20. Bui KH, von Appen A, DiGuilio AL, Ori A, Sparks L, Mackmull M-TT, Bock T, Hagen W, Andrés-Pons A, Glavy JS, Beck M. Integrated Structural Analysis of the Human Nuclear Pore Complex Scaffold. Cell. 2013; 155:1233–1243. [PubMed: 24315095]
21. von Appen A, Kosinski J, Sparks L, Ori A, DiGuilio AL, Vollmer B, Mackmull M-TT, Banterle N, Parca L, Kastritis P, Buczak K, Mosalaganti S, Hagen W, Andres-Pons A, Lemke EA, Bork P, Antonin W, Glavy JS, Bui KH, Beck M. *In Situ* Structural Analysis of the Human Nuclear Pore Complex. Nature. 2015; 526:140–143. [PubMed: 26416747]
22. Lin DH, Stuwe T, Schilbach S, Rundlet EJ, Perriches T, Mobbs G, Fan Y, Thierbach K, Huber FM, Collins LN, Davenport AM, Jeon YE, Hoelz A. Architecture of the Symmetric Core of the Nuclear Pore. Science. 2016; 352:aaf1015. [PubMed: 27081075]
23. Kosinski J, Mosalaganti S, von Appen A, Teimer R, DiGuilio AL, Wan W, Bui KH, Hagen WJ, Briggs JA, Glavy JS, Hurt E, Beck M. Molecular Architecture of the Inner Ring Scaffold of the Human Nuclear Pore Complex. Science. 2016; 352:363–365. [PubMed: 27081072]

24. Fernandez-Martinez J, Kim SJ, Shi Y, Upla P, Pellarin R, Gagnon M, Chemmama IE, Wang J, Nudelman I, Zhang W, Williams R, Rice WJ, Stokes DL, Zenklusen D, Chait BT, Sali A, Rout MP. Structure and Function of the Nuclear Pore Complex Cytoplasmic Mrna Export Platform. Cell. 2016; 167:1215. [PubMed: 27839866]
25. Alber F, Dokudovskaya S, Veenhoff LM, Zhang W, Kipper J, Devos D, Suprapto A, Karni-Schmidt O, Williams R, Chait BT, Rout MP, Sali A. Determining the Architectures of Macromolecular Assemblies. Nature. 2007; 450:683–694. [PubMed: 18046405]
26. Alber F, Dokudovskaya S, Veenhoff LM, Zhang W, Kipper J, Devos D, Suprapto A, Karni-Schmidt O, Williams R, Chait BT, Sali A, Rout MP. The Molecular Architecture of the Nuclear Pore Complex. Nature. 2007; 450:695–701. [PubMed: 18046406]
27. Amlacher S, Sarges P, Flemming D, van Noort V, Kunze R, Devos DP, Arumugam M, Bork P, Hurt E. Insight into Structure and Assembly of the Nuclear Pore Complex by Utilizing the Genome of a Eukaryotic Thermophile. Cell. 2011; 146:277–289. [PubMed: 21784248]
28. Fischer J, Teimer R, Amlacher S, Kunze R, Hurt E. Linker Nups Connect the Nuclear Pore Complex Inner Ring with the Outer Ring and Transport Channel. Nat. Struct. Mol. Biol. 2015; 22:774–781. [PubMed: 26344569]
29. Apelt L, Knockenhauer KE, Leksa NC, Benlasfer N, Schwartz TU, Stelzl U. Systematic Protein-Protein Interaction Analysis Reveals Intersubcomplex Contacts in the Nuclear Pore Complex. Mol. Cell. Proteomics. 2016; 15:2594–2606. [PubMed: 27194810]
30. Rout MP, Aitchison JD, Suprapto A, Hjertaas K, Zhao Y, Chait BT. The Yeast Nuclear Pore Complex: Composition, Architecture, and Transport Mechanism. J. Cell Biol. 2000; 148:635–651. [PubMed: 10684247]
31. Ori A, Banterle N, Iskar M, Andrés-Pons A, Escher C, Khanh Bui H, Sparks L, Solis-Mezarino V, Rinner O, Bork P, Lemke EA, Beck M. Cell Type-Specific Nuclear Pores: A Case in Point for Context-Dependent Stoichiometry of Molecular Machines. Mol. Syst. Biol. 2013; 9:648. [PubMed: 23511206]
32. Szymborska A, de Marco A, Daigle N, Cordes VC, Briggs JA, Ellenberg J. Nuclear Pore Scaffold Structure Analyzed by Super-Resolution Microscopy and Particle Averaging. Science. 2013; 341:655–658. [PubMed: 23845946]
33. Atkinson CE, Mattheyses AL, Kampmann M, Simon SM. Conserved Spatial Organization of FG Domains in the Nuclear Pore Complex. Biophys. J. 2013; 104:37–50. [PubMed: 23332057]
34. Fu G, Tu L-CC, Zilman A, Musser SM. Investigating Molecular Crowding within Nuclear Pores Using Polarization-PALM. eLife. 2017; 6
35. Bestembayeva A, Kramer A, Labokha AA, Osmanovic D, Liashkovich I, Orlova EV, Ford IJ, Charras G, Fassati A, Hoogenboom BW. Nanoscale Stiffness Topography Reveals Structure and Mechanics of the Transport Barrier in Intact Nuclear Pore Complexes. Nat. Nanotechnol. 2015; 10:60–64. [PubMed: 25420031]
36. Sakiyama Y, Mazur A, Kapinos LE, Lim RY. Spatiotemporal Dynamics of the Nuclear Pore Complex Transport Barrier Resolved by High-Speed Atomic Force Microscopy. Nat. Nanotechnol. 2016; 11:719–723. [PubMed: 27136131]
37. Labokha AA, Gradmann S, Frey S, Hülsmann BB, Urlaub H, Baldus M, Görlich D. Systematic Analysis of Barrier-Forming FG Hydrogels from *Xenopus* Nuclear Pore Complexes. EMBO J. 2013; 32:204–218. [PubMed: 23202855]
38. Rout MP, Aitchison JD, Magnasco MO, Chait BT. Virtual Gating and Nuclear Transport: The Hole Picture. Trends Cell Biol. 2003; 13:622–628. [PubMed: 14624840]
39. Lim RYH, Huang N-P, Köser J, Deng J, Lau AKH, Schwarz-Herion K, Fahrenkrog B, Aebi U. Flexible Phenylalanine-Glycine Nucleoporins as Entropic Barriers to Nucleocytoplasmic Transport. Proc. Natl. Acad. Sci. U.S.A. 2006; 103:9512–9517. [PubMed: 16769882]
40. Vovk A, Gu C, Opferman MG, Kapinos LE, Lim RY, Coalson RD, Jasnow D, Zilman A. Simple Biophysics Underpins Collective Conformations of the Intrinsically Disordered Proteins of the Nuclear Pore Complex. eLife. 2016; 5
41. Frey S, Richter RP, Görlich D. FG-Rich Repeats of Nuclear Pore Proteins Form a Three-Dimensional Meshwork with Hydrogel-Like Properties. Science. 2006; 314:815–817. [PubMed: 17082456]

42. Ader C, Frey S, Maas W, Schmidt HB, Görlich D, Baldus M. Amyloid-Like Interactions within Nucleoporin FG Hydrogels. Proc. Natl. Acad. Sci. U.S.A. 2010; 107:6281–6285. [PubMed: 20304795]
43. Eisele NB, Frey S, Piehler J, Görlich D, Richter RP. Ultrathin Nucleoporin Phenylalanine-Glycine Repeat Films and Their Interaction with Nuclear Transport Receptors. EMBO Rep. 2010; 11:366–372. [PubMed: 20379223]
44. Xu S, Powers M. A *In Vivo* Analysis of Human Nucleoporin Repeat Domain Interactions. Mol. Biol. Cell. 2013; 24:1222–1231. [PubMed: 23427268]
45. Eisele NB, Labokha AA, Frey S, Görlich D, Richter RP. Cohesiveness Tunes Assembly and Morphology of FG Nucleoporin Domain Meshworks - Implications for Nuclear Pore Permeability. Biophys. J. 2013; 105:1860–1870. [PubMed: 24138862]
46. Ribbeck K, Görlich D. Kinetic Analysis of Translocation through Nuclear Pore Complexes. EMBO J. 2001; 20:1320–1330. [PubMed: 11250898]
47. Peters R. Translocation through the Nuclear Pore: Kaps Pave the Way. Bioessays. 2009; 31:466–477. [PubMed: 19274657]
48. Yamada J, Phillips JL, Patel S, Goldfien G, Calestagne-Morelli A, Huang H, Reza R, Acheson J, Krishnan VV, Newsam S, Gopinathan A, Lau EY, Colvin ME, Uversky VN, Rexach MF. A Bimodal Distribution of Two Distinct Categories of Intrinsically Disordered Structures with Separate Functions in FG Nucleoporins. Mol. Cell. Proteomics. 2010; 9:2205–2224. [PubMed: 20368288]
49. Kapinos LE, Schoch RL, Wagner RS, Schleicher KD, Lim RY. Karyopherin-Centric Control of Nuclear Pores Based on Molecular Occupancy and Kinetic Analysis of Multivalent Binding with FG Nucleoporins. Biophys. J. 2014; 106:1751–1762. [PubMed: 24739174]
50. Koh J, Blobel G. Allosteric Regulation in Gating the Central Channel of the Nuclear Pore Complex. Cell. 2015; 161:1361–1373. [PubMed: 26046439]
51. Zahn R, Osmanovic D, Ehret S, Araya Callis C, Frey S, Stewart M, You C, Görlich D, Hoogenboom BW, Richter RP. A Physical Model Describing the Interaction of Nuclear Transport Receptors with FG Nucleoporin Domain Assemblies. eLife. 2016; 5
52. Schoch RL, Kapinos LE, Lim RY. Nuclear Transport Receptor Binding Avidity Triggers a Self-Healing Collapse Transition in FG-Nucleoporin Molecular Brushes. Proc. Natl. Acad. Sci. U.S.A. 2012; 109:16911–16916. [PubMed: 23043112]
53. Peleg O, Tagliazucchi M, Kroger M, Rabin Y, Szleifer I. Morphology Control of Hairy Nanopores. ACS Nano. 2011; 5:4737–4747. [PubMed: 21524134]
54. Osmanovic D, Bailey J, Harker AH, Fassati A, Hoogenboom BW, Ford IJ. Bistable Collective Behavior of Polymers Tethered in a Nanopore. Phys. Rev. E. 2012; 85:061917.
55. Li C, Goryaynov A, Yang W. The Selective Permeability Barrier in the Nuclear Pore Complex. Nucleus. 2016; 7:430–446. [PubMed: 27673359]
56. Jovanovic-Talisman T, Tetenbaum-Novatt J, McKenney AS, Zilman A, Peters R, Rout MP, Chait BT. Artificial Nanopores That Mimic the Transport Selectivity of the Nuclear Pore Complex. Nature. 2009; 457:1023–1027. [PubMed: 19098896]
57. Kowalczyk SW, Kapinos L, Blosser TR, Magalhaes T, van Nies P, Lim RY, Dekker C. Single-Molecule Transport across an Individual Biomimetic Nuclear Pore Complex. Nat. Nanotechnol. 2011; 6:433–438. [PubMed: 21685911]
58. Seeman NC, Sleiman HF. DNA Nanotechnology. Nat. Rev. Mater. 2017; 3:17068.
59. Rothemund PWK. Folding DNA to Create Nanoscale Shapes and Patterns. Nature. 2006; 440:297–302. [PubMed: 16541064]
60. Hong F, Zhang F, Liu Y, Yan H. DNA Origami: Scaffolds for Creating Higher Order Structures. Chem. Rev. 2017; 117:12584–12640. [PubMed: 28605177]
61. Xu W, Nathwani B, Lin C, Wang J, Karatekin E, Pincet F, Shih W, Rothman JE. A Programmable DNA Origami Platform to Organize Snares for Membrane Fusion. J. Am. Chem. Soc. 2016; 138:4439–4447. [PubMed: 26938705]
62. Derr ND, Goodman BS, Jungmann R, Leschziner AE, Shih WM, Reck-Peterson SL. Tug-of-War in Motor Protein Ensembles Revealed with a Programmable DNA Origami Scaffold. Science. 2012; 338:662–665. [PubMed: 23065903]

63. Hariadi RF, Sommese RF, Adhikari AS, Taylor RE, Sutton S, Spudich JA, Sivaramakrishnan S. Mechanical Coordination in Motor Ensembles Revealed Using Engineered Artificial Myosin Filaments. Nat. Nanotechnol. 2015; 10:696–700. [PubMed: 26149240]
64. Fu J, Liu M, Liu Y, Woodbury NW, Yan H. Interenzyme Substrate Diffusion for an Enzyme Cascade Organized on Spatially Addressable DNA Nanostructures. J. Am. Chem. Soc. 2012; 134:5516–5519. [PubMed: 22414276]
65. Shaw A, Lundin V, Petrova E, Fordos F, Benson E, Al-Amin A, Herland A, Blokzijl A, Hogberg B, Teixeira AI. Spatial Control of Membrane Receptor Function Using Ligand Nanocalipers. Nat. Methods. 2014; 11:841–846. [PubMed: 24997862]
66. Yang Q, Rout MP, Akey CW. Three-Dimensional Architecture of the Isolated Yeast Nuclear Pore Complex: Functional and Evolutionary Implications. Mol. Cell. 1998; 1:223–234. [PubMed: 9659919]
67. Denning DP, Rexach MF. Rapid Evolution Exposes the Boundaries of Domain Structure and Function in Natively Unfolded FG Nucleoporins. Mol. Cell. Proteomics. 2007; 6:272–282. [PubMed: 17079785]
68. Bailer SM, Balduf C, Hurt E. The Nsp1p Carboxy-Terminal Domain Is Organized into Functionally Distinct Coiled-Coil Regions Required for Assembly of Nucleoporin Subcomplexes and Nucleocytoplasmic Transport. Mol. Cell. Biol. 2001; 21:7944–7955. [PubMed: 11689687]
69. Bailer SM, Balduf C, Katahira J, Podtelejnikov A, Rollenhagen C, Mann M, Pante N, Hurt E. Nup116p Associates with the Nup82p-Nsp1p-Nup159p Nucleoporin Complex. J. Biol. Chem. 2000; 275:23540–23548. [PubMed: 10801828]
70. Israelachvili, JN. Intermolecular and Surface Forces. 3. Academic Press; Burlington, MA: 2011. p. 311-312.
71. Avakyan N, Conway JW, Sleiman HF. Long-Range Ordering of Blunt-Ended DNA Tiles on Supported Lipid Bilayers. J. Am. Chem. Soc. 2017; 139:12027–12034. [PubMed: 28783358]
72. Suzuki Y, Endo M, Sugiyama H. Lipid-Bilayer-Assisted Two-Dimensional Self-Assembly of DNA Origami Nanostructures. Nat Commun. 2015; 6:8052. [PubMed: 26310995]
73. Herold C, Schwille P, Petrov EP. DNA Condensation at Freestanding Cationic Lipid Bilayers. Phys. Rev. Lett. 2010; 104:148102. [PubMed: 20481965]
74. Popken P, Ghavami A, Onck PR, Poolman B, Veenhoff LM. Size-Dependent Leak of Soluble and Membrane Proteins through the Yeast Nuclear Pore Complex. Mol. Biol. Cell. 2015; 26:1386–1394. [PubMed: 25631821]
75. Timney BL, Raveh B, Mironska R, Trivedi JM, Kim SJ, Russel D, Wente SR, Sali A, Rout MP. Simple Rules for Passive Diffusion through the Nuclear Pore Complex. J. Cell Biol. 2016; 215:57–76. [PubMed: 27697925]
76. Kapinos LE, Huang B, Rencurel C, Lim R. Karyopherins Regulate Nuclear Pore Complex Barrier and Transport Function. J. Cell Biol. 2017; 216:3609–3624. [PubMed: 28864541]
77. Lowe AR, Tang JH, Yassif J, Graf M, Huang WY, Groves JT, Weis K, Liphardt JT. Importin-β Modulates the Permeability of the Nuclear Pore Complex in a Ran-Dependent Manner. eLife. 2015; 4
78. Tagliazucchi M, Peleg O, Kroger M, Rabin Y, Szleifer I. Effect of Charge, Hydrophobicity, and Sequence of Nucleoporins on the Translocation of Model Particles through the Nuclear Pore Complex. Proc. Natl. Acad. Sci. U.S.A. 2013; 110:3363–3368. [PubMed: 23404701]
79. Ghavami A, Veenhoff LM, van der Giessen E, Onck PR. Probing the Disordered Domain of the Nuclear Pore Complex through Coarse-Grained Molecular Dynamics Simulations. Biophys. J. 2014; 107:1393–1402. [PubMed: 25229147]
80. Jovanovic-Talisman T, Zilman A. Protein Transport by the Nuclear Pore Complex: Simple Biophysics of a Complex Biomachine. Biophys. J. 2017; 113:6–14. [PubMed: 28700925]
81. Lin C, Jungmann R, Leifer AM, Li C, Levner D, Church GM, Shih WM, Yin P. Submicrometre Geometrically Encoded Fluorescent Barcodes Self-Assembled from DNA. Nat. Chem. 2012; 4:832–839. [PubMed: 23000997]
82. Baddeley D, Cannell MB, Soeller C. Visualization of Localization Microscopy Data. Microsc. Microanal. 2010; 16:64–72. [PubMed: 20082730]

83. Leung C, Hodel AW, Brennan AJ, Lukoyanova N, Tran S, House CM, Kondos SC, Whisstock JC, Dunstone MA, Trapani JA, Voskoboinik I, Saibil HR, Hoogenboom BW. Real-Time Visualization of Perforin Nanopore Assembly. Nat. Nanotechnol. 2017; 12:467–473. [PubMed: 28166206]

84. Plimpton S. Fast Parallel Algorithms for Short-Range Molecular Dynamics. J. Comput. Phys. 1995; 117:1–19.

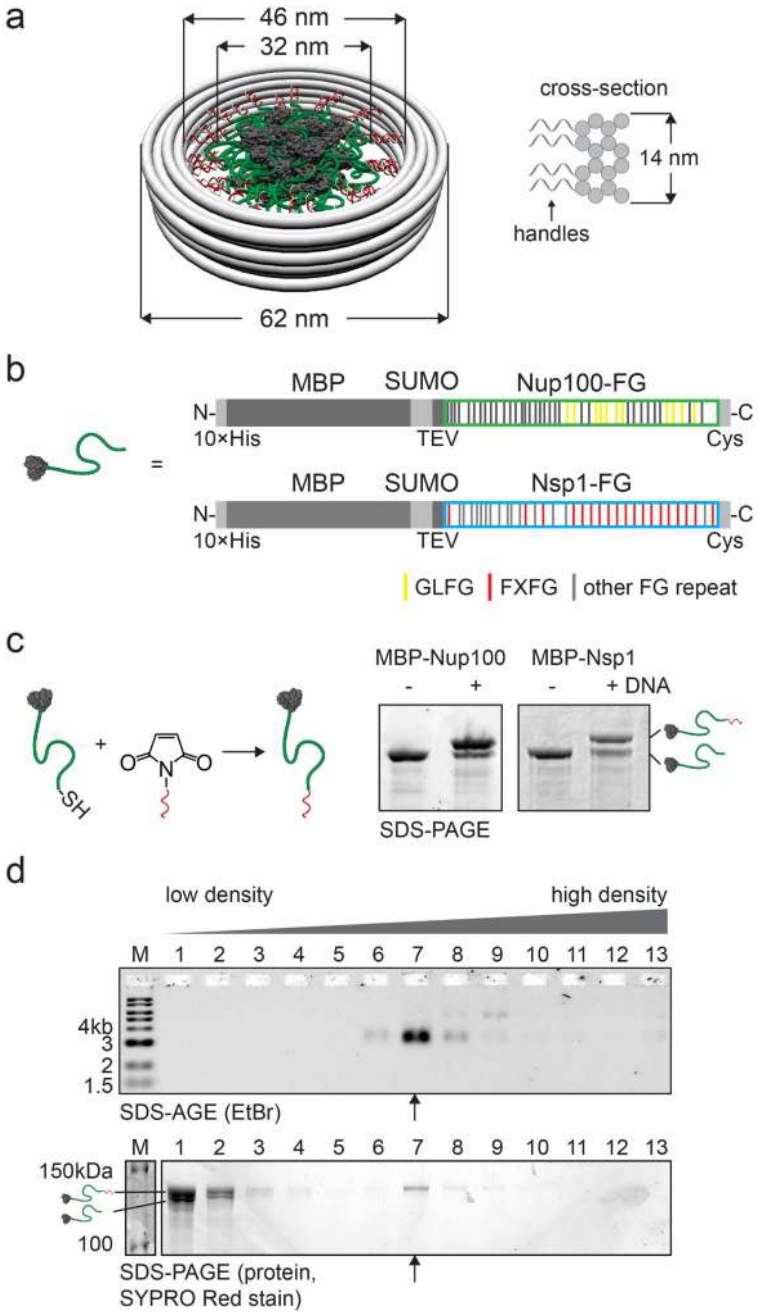

Figure 1.

Design and assembly of Nucleoporins Organized on DNA (NuPOD). (a) Cartoon and cross-section of the DNA origami cylinder with protruding inner DNA "handles" hybridized to DNA-labeled FG-nups (green, with red "anti-handles"). (b) MBP-Nup100-FG (a.a. 2-610) and MBP-Nsp1-FG (a.a. 2-603) protein constructs. FG-repeats are shown as vertical lines (with yellow, red, and grey lines representing GLFG repeats, FxFG repeats, and other FG-repeats, respectively). (c) Strategy for thiol-maleimide linkage between FG-nups and DNA, with SDS-PAGE showing the separation between proteins (−) and protein-DNA conjugates (+), proteins stained by SYPRO Red (left) or Coomassie (right). (d) Rate-zonal

centrifugation shows hybridized NuPODs enriched in fraction 7, denoted by arrow (M, molecular weight marker; top: SDS-agarose, EtBr stain; bottom: SDS-PAGE, SYPRO Red stain).

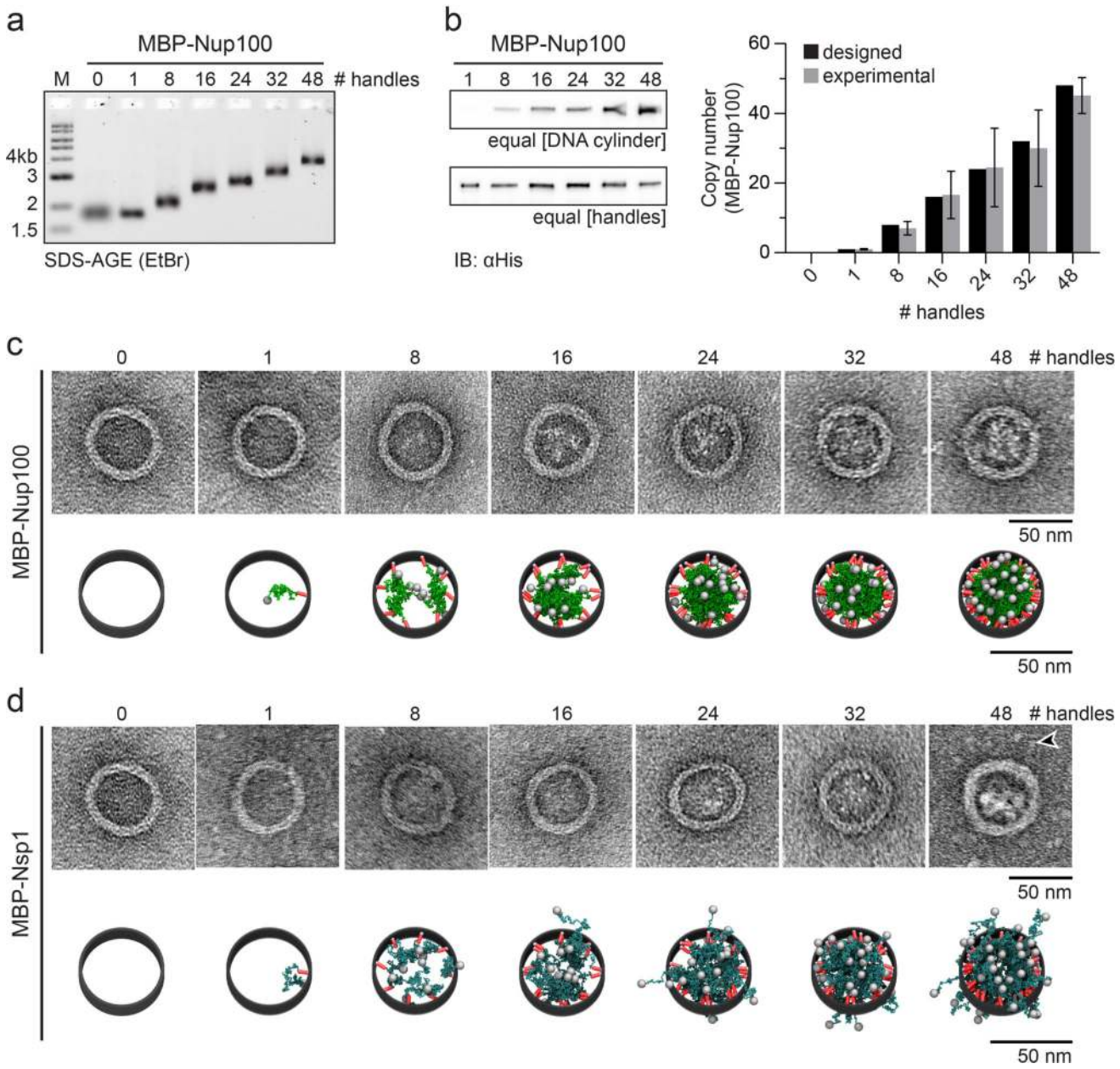

Figure 2.

Copy number and morphology of FG-domains inside NuPODs. (a) Step-wise mobility shift of NuPODs as the number of FG-domains increases (MBP-Nup100; M, molecular weight marker; SDS-agarose, EtBr stain). (b) Immunoblots (αHis) loaded with either equal amount of DNA cylinders or number of DNA handles, and quantification of copy numbers of MBP-Nup100 in NuPODs ($N = 4$ independent measurements for 1 and 8 handles, $N = 5$ for others; error bars show mean ± SD). See also Table S2. (c) Negative-stain TEM (top) showing appearance of protein clumps with increasing handle number in MBP-Nup100 NuPODs; snapshots of equilibrated molecular dynamics simulations (bottom) approximating the FG-domains as homogeneous polymers (green) with a sphere at their free ends representing MBP (light grey). The conjugated DNA handles are represented as straight rods (red). (d) As

panel c, for MBP-Nsp1, with arrowhead exemplifying a MBP moiety outside of ring and MBP-Nsp1 colored blue.

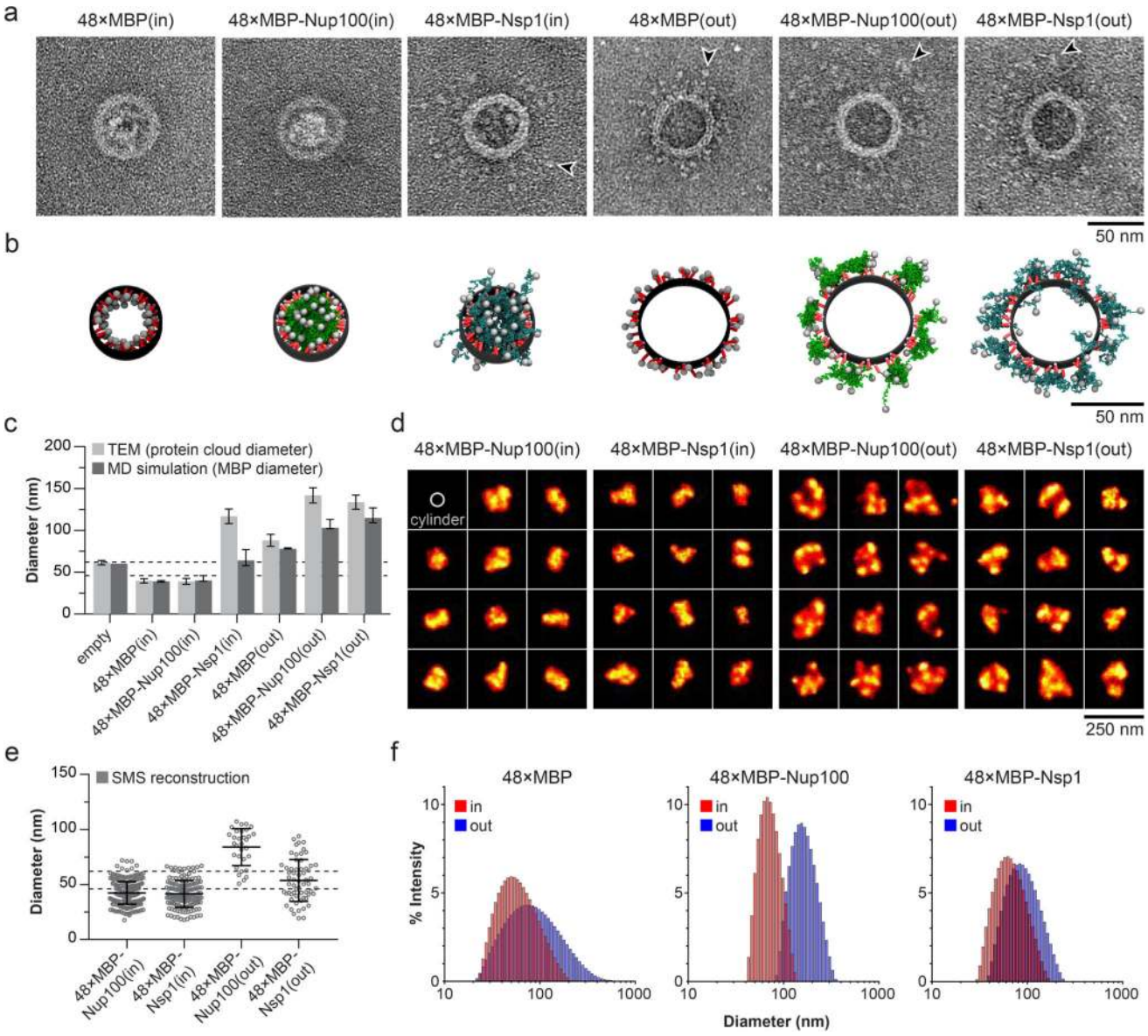

Figure 3.

Grafting of FG-domains on the inside or outside of NuPODs affects collective morphology. (a) Negative-stain TEM images showing indicated proteins in NuPODs; arrowheads show examples of MBP tags outside of NuPODs. (b) Snapshots of equilibrated molecular dynamics (MD) simulations of the corresponding inside and outside grafted NuPODs (with Nup100 and Nsp1 in green and blue, respectively, and grey spheres representing MBP; all MD snapshots are displayed at the same length scale; observed differences in diameter of the rings between the inside- and outside-grafted NuPODs reflect that only the inner and outer wall of the DNA ring are shown, respectively). (c) Measurements of protein extension by TEM and radial extent of MBP from the central axis in MD simulations for various NuPODs (dotted lines represent inner and outer walls of the DNA cylinder; TEM error bars show mean ± SD, $N = 96$ particles for 48×MBP(out), $N = 66$ for 48×MBP-Nsp1(out), $N = 100$ for others; MD shows diameter including 95% of MBP moeities, error bars show 90–99%). (d)

SMS reconstructions of individual NuPODs (only those with a minimum of 150 localizations shown). *En face* orientation of NuPODs was achieved by using biotin linkages on the bottom of the NuPOD to immobilize and position on a streptavidin-coated slide. For a spatial reference, we include a to-scale diagram of the DNA cylinder in the top left panel (grey). (e) Measured diameters from SMS reconstructions, after fitting with the model of a ring convolved with a 2D Gaussian (see SI; from left to right, N = 241, 144, 31, and 61; dotted lines represent inner and outer walls of the DNA cylinder; error bars show mean ± SD). (f) In-solution DLS measurements of NuPOD diameter, shown on logarithmic length scale.

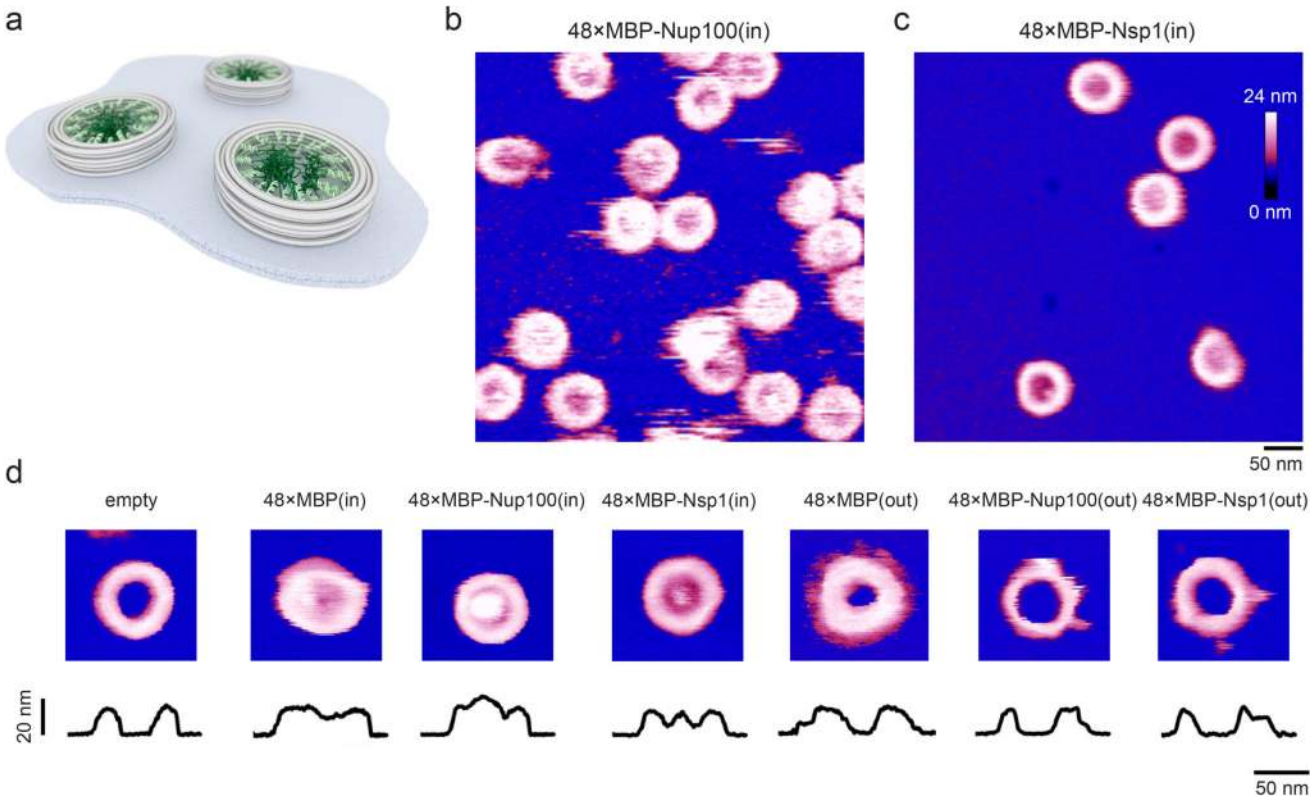

Figure 4.

AFM imaging of NuPODs in solution. (a) Schematic depicting NuPODs on top of a supported lipid bilayer. (b) AFM image of inside-grafted NuPODs with 48×MBP-Nup100, adsorbed on a supported DPPC:DDAB (3:1) bilayer. (c) As panel b, for 48×MBP-Nsp1. (d) Higher magnification AFM images and height profiles (as measured across the center of the pore) of different 48 handle NuPODs, showing an accumulation of protein inside and outside the DNA rings for the inside- and outside-grafted NuPODs, respectively. The images were acquired at 10–70 s per frame. Color scale, 0–24 nm.

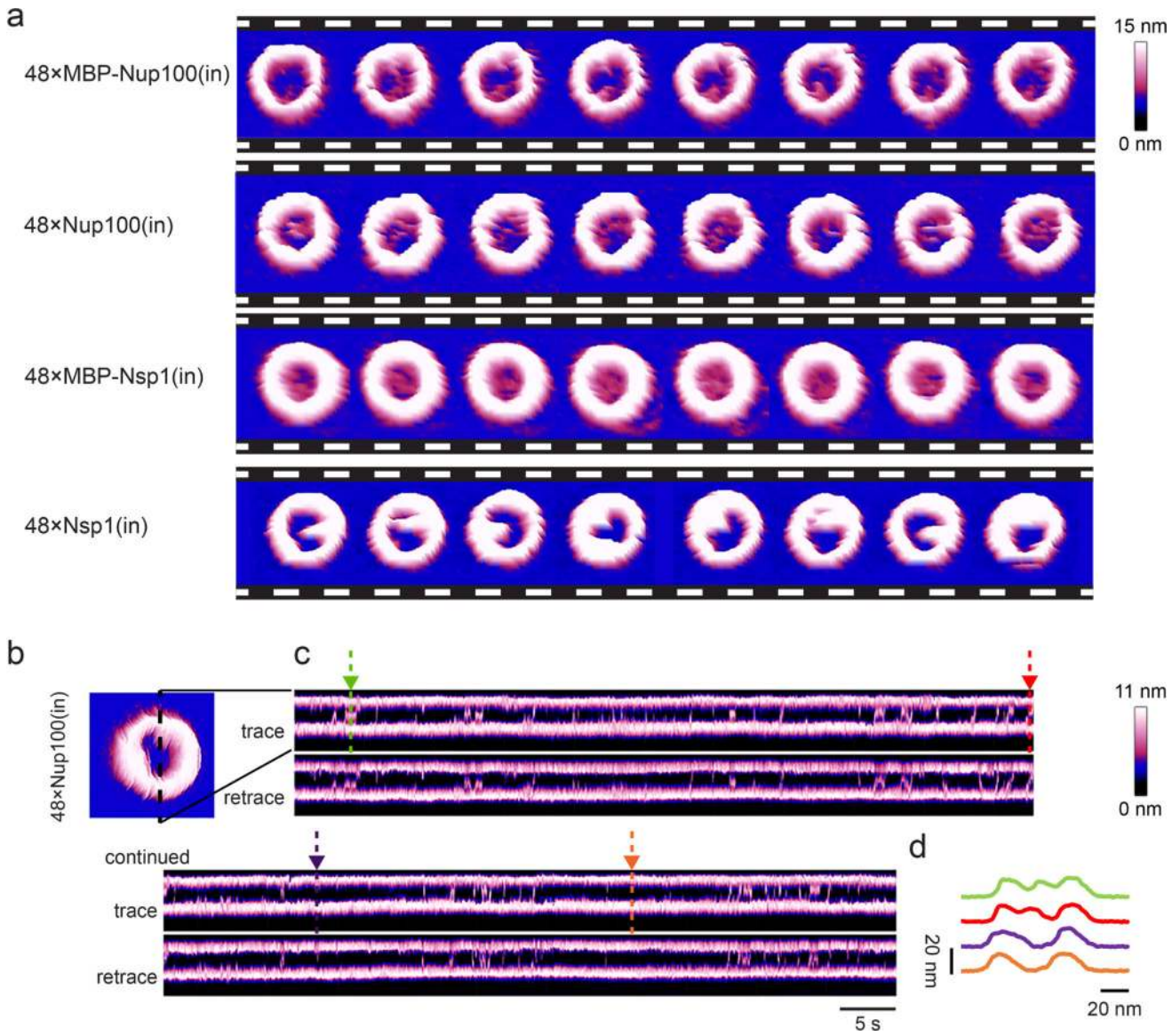

Figure 5.

Time-resolved imaging of FG-nup dynamics within NuPODs reveal transient molecular interactions. (a) Sequence of AFM images with 1.6 s between subsequent frames shown for an inside-grafted NuPOD with 48 copies of Nup100 and Nsp1, with and without the MBP moieties present. (b) AFM image of an inside-grafted 48×Nup100 NuPOD with MBP cleaved off (frame shown is at 13 s). The dashed line indicates where height profiles were recorded (on this same NuPOD) for the kymographs in c. (c) Kymographs showing the AFM height profile across the NuPOD as a function of time, with trace (top) and retrace (bottom) shown separately to validate the robustness of the observed fluctuations, and with 50 ms between subsequent scan lines. (d) Height profiles along positions indicated in c, showing 1–10 nm height variations in the NuPOD lumen as a function of time. Color scale, 0–15 nm (a,b), 0–11 nm (c).